

NUMERICAL RECOVERY OF SOURCE SINGULARITIES VIA THE RADIATIVE TRANSFER EQUATION WITH PARTIAL DATA

MARK HUBENTHAL

ABSTRACT. The inverse source problem for the radiative transfer equation is considered, with partial data. Here we demonstrate numerical computation of the normal operator $X_V^* X_V$ where X_V is the partial data solution operator to the radiative transfer equation. The numerical scheme is based in part on a forward solver designed by F. Monard and G. Bal. We will see that one can detect quite well the visible singularities of an internal optical source f for generic anisotropic k and σ , with or without noise added to the accessible data $X_V f$. In particular, we use a truncated Neumann series to estimate X_V and X_V^* , which provides a good approximation of $X_V^* X_V$ with an error of higher Sobolev regularity. This paper provides a visual demonstration of the authors' previous work in recovering the microlocally visible singularities of an unknown source from partial data. We also give the theoretical analysis necessary to justify the smoothness of the remainder when approximating the normal operator.

1. INTRODUCTION

The Radiative Transfer Equation (also sometimes referred to as the linear transport or linear Boltzmann equation) is often used to model the propagation of particles that exhibit absorption and scattering in various contexts, including the behavior of photons within biological tissues or of neutrons in a reactor. In this paper, we will consider an inverse problem relevant to optical molecular imaging (OMI), which is a physically safe imaging modality that has seen some recent advances in research. In this application, biochemical markers can be used to detect the presence of specific molecules or genes, and suitably designed markers could potentially identify diseases before phenotypical symptoms even appear. Such markers are typically light-emitting molecules, such as fluorophores or luminophores, which bind to the desired molecule to be detected. In contrast to Single Positron Emission Computed Tomography (SPECT), Positron Emission Tomography (PET), or Magnetic Resonance Imaging (MRI), optical markers emit low-energy near-infrared

Date: July 16, 2012.

2000 Mathematics Subject Classification. 35R30, 35Q60, 35S05.

Key words and phrases. Optical molecular imaging, radiative transfer equation, inverse problems, partial data.

photons that are relatively harmless to human tissue. Because of their low-energy level, the photons scatter before they are measured. Further specifics can be found in the bioengineering literature such as [6, 9, 16, 31, 32, 21].

The inverse problem we consider consists of reconstructing the spatial distribution of a radiative light source from measurements of outgoing photon intensities at the boundary of the medium. In many applications, the propagation of photons emitted can be modeled as inverse source problems of time-independent radiative transfer equations. We will assume that the optical parameters of the underlying medium are known, so that the problem of determining the source is feasible. In practice, such optical parameters do not vary too much in biological tissue, and not knowing their true values does not significantly effect one's ability to detect edges in the image. It is shown in [29] that under mild assumptions on the scattering and absorption parameters of the medium this is possible. Other work on the inverse source problem for the RTE under varying assumptions can be found in [4, 3, 26, 22, 17], and further background on optical tomography can be found in [28, 1]. In the case of partial data, [15] shows that one can recover the *visible* singularities of the source f , which is a particular subset of $\text{WF}(f)$. As such, the primary focus of this paper is to provide a numerical scheme by which to detect such singularities. We now describe more precisely the mathematical problem.

We assume Ω to be a bounded domain in \mathbb{R}^n with smooth boundary and outer unit normal vector $\nu(x)$. As in [29, 15], we also assume that the data is given on the boundary of a larger strictly convex domain $\Omega_1 \supset \Omega$. The radiative transfer equation on the domain Ω with internal source f and zero incoming illuminations is given by

$$(1.1) \quad \begin{aligned} \theta \cdot \nabla_x u(x, \theta) + \sigma(x, \theta)u(x, \theta) - \int_{\mathbb{S}^{n-1}} k(x, \theta, \theta')u(x, \theta') d\theta' &= f(x), \\ u|_{\partial_- S\Omega} &= 0, \end{aligned}$$

where the absorption σ and the collision kernel k are functions with regularity specified later, the solution $u(x, \theta)$ gives the intensity of photons at x moving in the direction θ , and $\partial_{\pm} S\Omega$ is the set of points $(x, \theta) \in \partial\Omega \times \mathbb{S}^{n-1}$ such that $\pm\nu(x) \cdot \theta > 0$. That is, $\partial_{\pm} S\Omega$ is the set of points $(x, \theta) \in \partial\Omega \times \mathbb{S}^{n-1}$ such that θ is pointing outward or inward, respectively. The source term f will be assumed to depend on x only for our purposes. We also recall, given the physical model, that equation 1.1 is only applicable at a single frequency, as the parameters σ and k typically vary widely with different frequencies. It is also important that the photons' energy be relatively low, since for high energy photons each scattering event is often accompanied by an energy change. This is discussed briefly in [15], and we mention it primarily to point out the limitations imposed by the assumptions of the model.

In the case of full data, we have boundary measurements

$$(1.2) \quad Xf(x, \theta) = u|_{\partial_+ S\Omega}.$$

In [29], it is shown that for an open, dense set of absorption and scattering coefficients $(\sigma, k) \in C^2(\overline{\Omega} \times \mathbb{S}^{n-1}) \times C^2(\overline{\Omega} \times \mathbb{S}^{n-1} \times \mathbb{S}^{n-1})$, one can recover $f \in L^2(\Omega)$ uniquely from boundary measurements Xf on all of $\partial_+ S\Omega$. To set up the case of partial data, first let $V \subset \partial_+ S\Omega$ be open and let $\tilde{V} \Subset V$. Let $\chi_V \in C_0^\infty(\partial_+ S\Omega)$ be a smooth cutoff function such that $\chi_V(x, \theta) \equiv 1$ for $(x, \theta) \in \tilde{V}$ and $\chi_V(x, \theta) \equiv 0$ for $(x, \theta) \notin V$. The boundary measurements are then given by

$$(1.3) \quad X_V f(x, \theta) = \chi_V(x, \theta) u|_{\partial_+ S\Omega}.$$

To make notation a bit simpler, if $V = \partial_+ S\Omega$ (complete data) we will just write X , since in this case $X_V = X$.

We now consider the complementary problem of numerical computation of solutions to (1.1) and using the accessible part of the synthesized data to visualize the results of [15]. To this end, we employ a technique from [19] that uses rotations applied to the parameters in the spectral domain to help eliminate the ray effect, which is a byproduct of the discrete ordinates method. It should be noted that in principle such a method could be applied in any dimension, but for the actual computations we will restrict ourselves to the two dimensional case. We also refer the reader to [12] for another approach to solving the direct transport equation using finite element methods, which we do not use here.

Our main goal is to approximate the operators X^*Xf and $X_V^*X_Vf$ in the two-dimensional case. Ignoring the technical details for the moment, the idea is to utilize a Neumann series to approximate the forward solution operator X_V and its adjoint X_V^* . As such, one must truncate the series to a finite number of terms when computing $X_V^*X_V$, and the difference of the approximation from the true function $X_V^*X_Vf$ will have some (higher) Sobolev regularity. The only theoretical result herein is Lemma 2.3, which essentially asserts that, if m_1 terms are computed in the approximation of X and m_2 terms are computed in the approximation of X^* , then $[X^*X]_{\text{approx}}f - X^*Xf \in H^{l+m+1}(\Omega)$, where $m = \min\{m_1, m_2\}$ and $f \in H^l(\Omega)$.

In Section 2, we review the background related to recovering the visible singularities of a source f given partial data of its outgoing intensity on the boundary. This is summarized by Theorem 2.2 and Corollary 6.4 of [15]. In Section 3 we describe the algorithm used to compute the forward solution u to (1.1). Following, in Section 4 we detail the similar approach used to approximate X_V^* . Finally, we present some numerical computations for a few different types of sources with and without noise added to X_Vf in Section 6. Section 5 proves the main technical estimate of this work, and Appendix A provides some necessary results for iterated weakly singular-type integral operators.

2. BACKGROUND AND STATEMENT OF MAIN LEMMA

Let us establish some standard notation. We set

$$(2.1) \quad T_0 = \theta \cdot \nabla_x, \quad T_1 = T_0 + \sigma, \quad T = T_0 + \sigma - K,$$

where σ denotes the operation of multiplication by $\sigma(x, \theta)$, and K is defined by

$$(2.2) \quad Kf(x, \theta) = \int_{\mathbb{S}^{n-1}} k(x, \theta, \theta') f(x, \theta') d\theta'.$$

In order to compute the normal operator $X_V^* X_V f$, we first need to generate the solution to the radiative transport equation (1.1), given by

$$\begin{aligned} u &= T_1^{-1}(\text{Id} - KT_1^{-1})^{-1} Jf \\ &= T_1^{-1} \sum_{m=0}^{\infty} (KT_1^{-1})^m Jf. \end{aligned}$$

If we set $u_0(x, \theta) := [T_1^{-1}f](x, \theta)$ and set $u_l := T_1^{-1}Ku_{l-1}$ for $l \geq 1$, then $u = \sum_{l \geq 0} u_l$. In practice, it is quite simple to compute the scattering term Ku_{l-1} at each iteration. In order to compute T_1^{-1} we will use a simple first order Euler method to solve the associated differential equation to which T_1^{-1} is the solution operator:

$$\begin{aligned} \theta \cdot \nabla_x u(x, \theta) + \sigma(x, \theta)u(x, \theta) &= g(x, \theta), \quad (x, \theta) \in \Omega \times \mathbb{S}^{n-1} \\ u|_{\partial_- S\Omega} &\equiv 0. \end{aligned}$$

For a given source $f \in L^2(\Omega)$, recall the *microlocally visible set* corresponding to partial measurements on $\partial_+ S\Omega_1$, given by

$$(2.3) \quad \mathcal{M}' := \{(x, \xi) \in T^*\Omega \mid \exists \theta \in \mathbb{S}^{n-1} \text{ such that } \theta \cdot \xi = 0 \text{ and } \chi_V^\#(x, \theta) \neq 0\}.$$

Here $\chi_V^\#(x, \theta)$ is the extension of $\chi_V : \partial_+ S\Omega_1 \rightarrow \mathbb{R}$ to $\Omega_1 \times \mathbb{S}^{n-1}$ defined by $\chi_V^\#(x, \theta) = \chi_V(x + \tau_+(x, \theta)\theta, \theta)$.

We restate the main result of [15] for recovering singularities of a general L^2 source with partial data:

Theorem 2.1 ([15], Theorem 2.2). *Let l be a positive integer. There exists an open dense set \mathcal{O}_l of pairs $(\sigma, k) \in C^\infty(\overline{\Omega} \times \mathbb{S}^{n-1}) \times C^\infty(\overline{\Omega}_x \times \mathbb{S}_{\theta'}^{n-1} \times \mathbb{S}_\theta^{n-1})$ depending on l such that given $(\sigma, k) \in \mathcal{O}_l$, if $(z, \xi) \in \mathcal{M}'$, then there exists a function $v \in H^l(\Omega)$ such that*

$$(2.4) \quad (z, \xi) \notin WF(X_V^* X_V f) \implies (z, \xi) \notin WF(f + v).$$

The following corollary applies when $\|KT_1^{-1}\|$ has small enough norm as an operator from $L^2(\Omega \times \mathbb{S}^{n-1}) \rightarrow L^2(\Omega \times \mathbb{S}^{n-1})$.

Corollary 2.2 ([15], Corollary 6.4). *Suppose that $\|KT_1^{-1}\| < 1$. Then in Theorem 2.1 we have $v = 0$.*

With this in mind, we can state the main theoretical estimate of this work, which justifies our approach in the numerical computations. The proof is given in Section 5.

Lemma 2.3. *Suppose $f \in H^l(\Omega)$ and $\sigma, k \in C^\infty$. Let $m_1, m_2 \geq 0$. Then*

$$X_V^* X_V f - \sum_{j=0}^{m_2} \sum_{i=0}^{m_1} [\chi_V R_+ T_1^{-1} (K T_1^{-1})^j J]^* \chi_V R_+ T_1^{-1} (K T_1^{-1})^i J f \in H^{l+m+1}(\Omega_1)$$

where $m = \min\{m_1, m_2\}$.

3. NUMERICAL METHOD FOR THE DIRECT PROBLEM

We now present a detailed summary of the method used to solve (1.1) for $n = 2$. Note that at this stage it is not important that the source f be isotropic, but such an assumption will be used when computing the normal operator later on. As in [19] we use the source iteration method, which requires one to solve problems of the form

$$(3.1) \quad \begin{aligned} \theta \cdot \nabla_x u + \sigma(x, \theta) u &= g(x, \theta) \\ u|_{\partial_- S\Omega} &= 0. \end{aligned}$$

Without loss of generality, we may take $\Omega = \mathbb{D} \subset \mathbb{R}^2$ where \mathbb{D} is the unit disk, and assume that σ, k and f are all supported compactly in $\mathbb{D} \times \mathbb{S}^1$ or \mathbb{D} as appropriate. Such an assumption can be justified by finding a ball $B(0, R)$ large enough and rescaling the coordinates accordingly. The main advantage here from a numerical standpoint is that Ω remains invariant under rotations. Now, for actually computing T_1^{-1} , it will be easier to have boundary conditions on a cartesian domain. To that end, for each $\eta \in (0, 2\pi)$ denote $\theta = \theta(\eta) = (\cos(\eta), \sin(\eta))$ and let $\theta^\perp = \theta(\eta)^\perp$ be the counterclockwise rotation of θ by $\pi/2$. That is $\theta(\eta)^\perp = (-\sin \eta, \cos \eta)$. For each $\eta \in (0, 2\pi)$ define the η -dependent square

$$C_\eta = \{x \in \mathbb{R}^2 \text{ such that } |x \cdot \theta| < 1 \text{ and } |x \cdot \theta^\perp| < 1\}.$$

In short, C_η is the square of side length 2 rotated by an angle η . The corresponding incoming and outgoing sets (analogous to $\partial_\pm S\Omega$) are given by

$$\Gamma_{\pm, \eta} = \{x \in \partial C_\eta \text{ such that } x \cdot \theta = \pm 1 \text{ and } |x \cdot \theta^\perp| < 1\}.$$

At the heart of the rotational method, we perform a rotational change coordinates so that the derivative in the direction θ becomes ∂_x . Fix an angle η and for $x = (\mathbf{x}, \mathbf{y}) \in [-1, 1]^2$ define

$$(3.2) \quad u_\eta(\mathbf{x}, \mathbf{y}) = [u]_\eta(\mathbf{x}, \mathbf{y}) := u(\mathbf{x} \cos \eta - \mathbf{y} \sin \eta, \mathbf{x} \sin \eta + \mathbf{y} \cos \eta, \eta)$$

$$(3.3) \quad v_\eta(\mathbf{x}, \mathbf{y}) = [v]_\eta(\mathbf{x}, \mathbf{y}) := v(\mathbf{x} \cos \eta - \mathbf{y} \sin \eta, \mathbf{x} \sin \eta + \mathbf{y} \cos \eta)$$

where u, v are functions on \mathbb{R}^2 and $\mathbb{R}^2 \times \mathbb{S}^1$, respectively. The bracket notation will only be used for functions which already have a subscript. With

this change of variables, we can rewrite (3.1) as

$$(3.4) \quad \begin{aligned} \frac{\partial}{\partial x_1} u_\eta(\mathbf{x}, \mathbf{y}) + \sigma_\eta(\mathbf{x}, \mathbf{y}) u_\eta(\mathbf{x}, \mathbf{y}) &= g_\eta(\mathbf{x}, \mathbf{y}), \\ u_\eta(-1, \mathbf{y}) &= 0 \quad \text{on } \Gamma_{-, \eta} \end{aligned}$$

We remark that for a general (possibly non-zero) function $h \in L^1(\partial_- S\mathbb{D})$, we would have the boundary condition \tilde{h}_η on $\Gamma_{-, \eta}$, obtained by projecting h onto $\Gamma_{-, \eta}$ via the relation $\tilde{h}_\eta(x_1, x_2) = h(P_-^{-1}(x_1, x_2, \eta))$, where

$$P_\pm : \partial_\pm S\mathbb{D} \ni (x, \eta) \mapsto P_\pm(x, \eta) = \pm\theta(\eta) - \det(x, \theta(\eta))\theta(\eta)^\perp \in \Gamma_{\pm, \eta}.$$

Since the measurements are necessarily discrete, we introduce the fixed parameters N_x , N_d and N_{scat} to represent the number of grid points in each spatial dimension, the number of directions measured, and the number of scattering terms computed in the series $T_1^{-1} \sum_{m=0}^{\infty} (KT_1^{-1})^m J$, respectively. Typically, we will take each such parameter to be a power of 2, since FFT algorithms are used to rotate the grids. Then the basic idea for computing T_1^{-1} is to solve equations of the type (3.4) by first computing g_η and σ_η by rotating the images of $\sigma(\cdot, \eta)$ and $g(\cdot, \eta)$ clockwise by the angle η in the x variable. Then we solve (3.4) for u_η , which can be done, for example, by using a simple first order Euler method along each column of the cartesian grid. Specifically, denote $s_x := \frac{2}{N_x}$, we set $u_\eta(x_1, \cdot) = 0$ and consider the cartesian grid $\{\mathbf{x}_1, \dots, \mathbf{x}_{N_x}\} \otimes \{\mathbf{y}_1, \dots, \mathbf{y}_{N_x}\}$ where $\mathbf{x}_i, \mathbf{y}_i = -1 + (i - \frac{1}{2})s_x$ for $1 \leq i \leq N_x$. Then the Euler method would give the update

$$u_\eta(x_j, \mathbf{y}) = u_\eta(x_{j-1}, \mathbf{y}) + s_x (g_\eta(x_{j-1}, \mathbf{y}) - \sigma_\eta(x_{j-1}, \mathbf{y}) u_\eta(x_{j-1}, \mathbf{y})), \quad 2 \leq j \leq N_x.$$

In order to compute K , we define the angular step size $\delta := \frac{2\pi}{N_d}$ and sum over the set of angles $\{\eta_1, \dots, \eta_{N_d}\}$ where $\eta_i = (1 - \frac{1}{2})\delta$. We can then approximate K by the discrete operator K_δ which has the formula

$$(3.5) \quad K_\delta g(\mathbf{x}, \eta_i) = \delta \sum_{j=1}^{N_d} g(\mathbf{x}, \eta_j) k(\mathbf{x}, \eta_j, \eta_i), \quad 1 \leq i \leq N_d.$$

3.1. Computing X_V . We describe in Algorithm 1 the iterative scheme to numerically solve (1.1) and simulate the partial data $X_V f$ with respect to some subset $V \subset \partial_+ S\Omega$.

What we have not yet described in much detail is the method used to compute the rotations of each function, which we discuss briefly within the remaining portion of this section. For more details however, we refer the reader to [19]. The general idea is to write the rotation map $r_\eta(\mathbf{x}, \mathbf{y}) = (\mathbf{x} \cos \eta + \mathbf{y} \sin \eta, -\mathbf{x} \sin \eta + \mathbf{y} \cos \eta)$ as a composition of dilations and shearing/slant operations in each variable separately. In particular, we can write

$$\begin{aligned} r_\eta &= d_{\mathbf{x}, \frac{1}{\cos \eta}} \circ s_{\mathbf{x}, -\sin \eta} \circ d_{\mathbf{y}, \cos \eta} \circ s_{\mathbf{y}, \tan \eta}, \\ s_{\mathbf{y}, \alpha}(\mathbf{x}, \mathbf{y}) &= (\mathbf{x}, \mathbf{y} - \alpha \mathbf{x}), & s_{\mathbf{x}, \beta}(\mathbf{x}, \mathbf{y}) &= (\mathbf{x} - \beta \mathbf{y}, \mathbf{y}), & \alpha, \beta &\in \mathbb{R} \\ d_{\mathbf{x}, t}(\mathbf{x}, \mathbf{y}) &= (t\mathbf{x}, \mathbf{y}), & d_{\mathbf{y}, t}(\mathbf{x}, \mathbf{y}) &= (\mathbf{x}, t\mathbf{y}), & t &\in \mathbb{R}. \end{aligned}$$

Algorithm 1 Computing $X_V f$

```

1: Let  $u_0$  solve  $\theta \cdot \nabla u + \sigma u = f$ 
2: for  $i = 1$  to  $N_d$  do
3:   compute  $\sigma_{\eta_i}$  and  $f_{\eta_i}$ 
4:   solve  $\partial_{x_1}[u_0]_{\eta_i} + \sigma_{\eta_i}[u_0]_{\eta_i} = f_{\eta_i}$  for  $[u_0]_{\eta_i}$ 
5:    $u_0(\mathbf{x}, \mathbf{y}, \eta_i) \leftarrow [[u_0]_{\eta_i}]_{-\eta_i}(\mathbf{x}, \mathbf{y})$ 
6: end for
7: for  $j = 1$  to  $N_{\text{scat}}$  do
8:    $f_j \leftarrow K_\delta u_{j-1}$ 
9:   for  $i = 1$  to  $N_d$  do
10:    compute  $[f_j]_{\eta_i}$ 
11:    solve  $\partial_{x_1}[u_j]_{\eta_i} + \sigma_{\eta_i}[u_j]_{\eta_i} = [f_j]_{\eta_i}$  for  $[u_j]_{\eta_i}$ 
12:     $u_j(\mathbf{x}, \mathbf{y}, \eta_i) \leftarrow [[u_j]_{\eta_i}]_{-\eta_i}(\mathbf{x}, \mathbf{y})$ 
13:   end for
14: end for
15:  $u \leftarrow \sum_{j=0}^{N_{\text{scat}}} u_j$ 
16: compute  $\chi_V u \Big|_{\partial_+ S\mathbb{D}}$ 

```

The shearing/slant operations $s_{\mathbf{x},\beta}$ and $s_{\mathbf{y},\alpha}$ are implemented in phase space using a periodic interpolation function together with some identities utilizing the discrete forward and inverse Fourier transform. Specifically, we first embed the $N_x \times N_x$ image into a $2N_x \times N_x$ image, padding the top and bottom of the image with $\frac{N_x}{2} \times N_x$ arrays of zeros. We then perform the vertical shearing operation $s_{\mathbf{y},\alpha}$, which independently shifts each column of the image by an amount that depends linearly on the column index with factor $-\alpha$.

The operation of shifting a vector $x = [x_1, \dots, x_m]^T$ by an amount s is done in phase space. First we define the $2m$ -periodic function

$$(3.6) \quad D_m(y) = \frac{\sin(\pi y)}{m \sin\left(\frac{\pi y}{m}\right)}, \quad y \in \mathbb{R}.$$

We then define the spectral interpolant

$$(3.7) \quad \tilde{x}(y) := \sum_{l=1}^m x_l D_m(y - l),$$

which coincides with x_j when $y = j$ and interpolates between those values sinusoidally (see Figure 1). The spectrally shifted vector x_s is given by

$$x_s = [\tilde{x}(1+s), \tilde{x}(2+s), \dots, \tilde{x}(m+s)]^T.$$

Note that x_s is not a priori defined for $s \in \mathbb{Z}$, but it can be extended continuously to such points due to the structure of the singularities of D_m .

Now, in practice we have first padded the image above and below with zeros, so we have $m = 2N_x$ which is even. It is then straightforward to verify

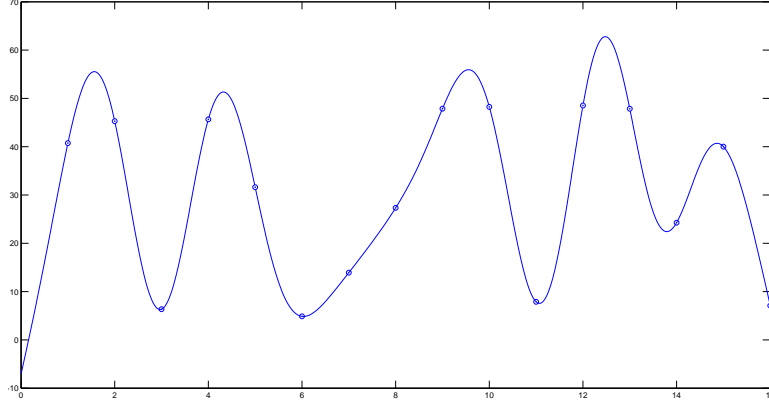


FIGURE 1. The values of a random 16-vector x are plotted while overlaid with the spectral interpolant $\tilde{x}(y) = \sum_{l=1}^m x_l D_m(y-l)$ for $y \in [0, 16]$.

that

$$D_{2N_x}(t) = \frac{\sin(\pi t)}{2N_x \sin \frac{\pi t}{2N_x}} = \frac{1}{2N_x} \sum_{l=-N_x}^{N_x-1} e^{i \frac{\pi}{N_x} (l+\frac{1}{2})t}, \quad t \in [0, 2N_x].$$

Recall the N -point discrete Fourier and inverse Fourier transforms, given by

$$X(k) = F_{j \rightarrow k}^N[x(j)] = \sum_{j=1}^N x(j) e^{-\frac{2\pi i}{N}(j-1)(k-1)}, \quad k = 1, \dots, N,$$

$$x(j) = F_{k \rightarrow j}^{-1,N}[X(k)] = \frac{1}{N} \sum_{k=1}^N X(k) e^{2\pi i N(j-1)(k-1)}, \quad j = 1, \dots, N.$$

It is then possible to write $\tilde{x}(l-s)$ for $l = 1, \dots, 2N_x$ as a composition of discrete Fourier transforms and inverse transforms and multiplication by complex exponentials. In particular,

$$(3.8) \quad \tilde{x}(l-s) = e^{i \frac{\pi}{N_x} (-N_x + \frac{1}{2})(l-1)} F_{k \rightarrow l}^{-1, 2N_x} \left[e^{-i \frac{\pi}{N_x} (k-1-N_x + \frac{1}{2})s} F_{j \rightarrow k}^{2N_x} \left[x(j) e^{-i \frac{\pi}{N_x} (-N_x + \frac{1}{2})(j-1)} \right] \right].$$

The dilation operations $d_{\mathbf{x},t}$ and $d_{\mathbf{y},t}$ are computed via a resampling done in the Fourier domain. In particular, we must resample a vector x of size $2N_x$ down to a vector \bar{x} of size N_x but with a different step size. We can do this by using the N -point fractional Fourier transform with coefficient α , defined by

$$(3.9) \quad X(l) = G_{k \rightarrow l}^{N,\alpha}[x] = \sum_{k=1}^N x(k) e^{-2\pi i \alpha (k-1)(l-1)}.$$

For example, if we start with a vector x sampled at the gridpoints $\{j-1\}_{j=1}^{2m}$ and we want to shift x by s (i.e. sample at $\{j-1+s\}_{j=1}^{2m}$) and then resample

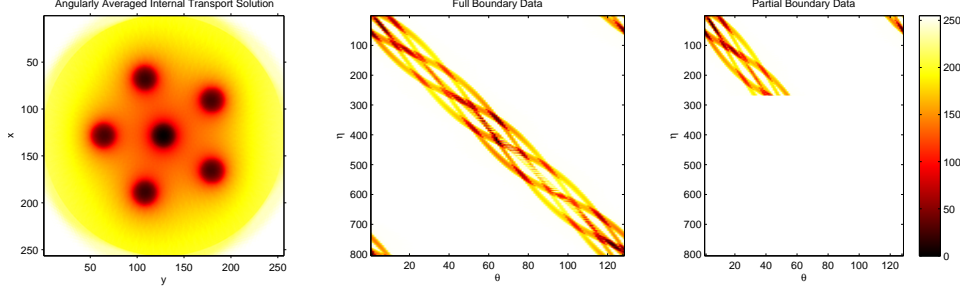


FIGURE 2. The angularly averaged solution to (1.1) corresponding to the internal source given in Figure 3 (left). The other two images show the complete and partial data Xf and $X_V f$, respectively, where V is the outgoing conic set above the arc of $\partial\mathbb{D}$ defined by $\eta \in [0, \pi/3]$. The axes are labeled such that θ is the transport direction and η is the position along the boundary $\partial\mathbb{D}$, with $\eta = 0$ corresponding to the point $(1, 0)$.

back to a vector \bar{x} taking values at the m points $y_l = s + h(l-1)$ for $l = 1, \dots, m$, then

$$(3.10) \quad \bar{x}(y_l) = \frac{1}{2m} e^{i\frac{\pi}{m}(-m+\frac{1}{2})h(l-1)} G_{k \mapsto l}^{2m, \frac{-h}{2m}} \left[e^{i\frac{\pi}{m}(k-m-1+\frac{1}{2})s} F_{j \mapsto k}^{2m} \left[x(j) e^{-i\frac{\pi}{m}(-m+\frac{1}{2})(j-1)} \right] \right].$$

This corresponds to a vertical dilation composed with a vertical shift (see [2, 19]).

4. APPROXIMATING THE NORMAL OPERATOR $X_V^* X_V$

After approximating the solution to the forward problem and restricting to $\partial_+ S\Omega$ to obtain the simulated data Xf , we can then proceed with computing $X^* Xf$, and similarly, $X_V^* X_V f$. Recall that for any $N \in \mathbb{N}$

$$\begin{aligned} X_V f &= \chi_V R_+ T_1^{-1} (\text{Id} - K T_1^{-1})^{-1} J f \\ &= \chi_V R_+ T_1^{-1} \sum_{m=0}^N (K T_1^{-1})^m J f + \chi_V R_+ T_1^{-1} (K T_1^{-1})^{N+1} (\text{Id} - K T_1^{-1})^{-1} J f. \end{aligned}$$

Under the condition that $\|K T_1^{-1}\|_{L^2 \rightarrow L^2} < 1$, we then have

$$(4.1) \quad X_V^* = J^* \left(\sum_{m=0}^{\infty} ([T_1^{-1}]^* K^*)^m \right) [\chi_V R_+ T_1^{-1}]^*$$

To numerically compute X_V^* , we separately compute the three types of terms appearing in (4.1).

Given that $J : L^2(\Omega) \rightarrow L^2(\Omega \times \mathbb{S}^{n-1})$, it is straightforward to verify that

$$(4.2) \quad J^*g(x) = \int_{\mathbb{S}^{n-1}} g(x, \theta) d\theta.$$

We also compute

$$(4.3) \quad K^*g(x, \theta) = \int_{\mathbb{S}^{n-1}} k(x, \theta', \theta) g(x, \theta') d\theta'.$$

In the isotropic scattering case, this gives

$$(4.4) \quad K^*g(x, \theta) = k(x) \int_{\mathbb{S}^{n-1}} g(x, \theta') d\theta'.$$

We will need the discretized version of (4.3) in the same vain as (3.5), which is given by

$$(4.5) \quad K_\delta^*g(x, \eta_i) = \delta \sum_{j=1}^{N_d} k(x, \eta_j, \eta_i) g(x, \eta_j), \quad 1 \leq i \leq N_d$$

One can also verify that $T_1^{-1} : L^2(\Omega \times \mathbb{S}^{n-1}) \rightarrow L^2(\Omega \times \mathbb{S}^{n-1})$ has adjoint

$$(4.6) \quad [T_1^{-1}]^*g(x, \theta) = \int_0^\infty \exp\left(-\int_0^s \sigma(x + \tau\theta, \theta) d\tau\right) g(x + s\theta, \theta) ds.$$

However, in order to apply $[T_1^{-1}]^*$ numerically, it is easier to use the associated first order differential equation for which it is the solution operator. We already know that T_1^{-1} is a left inverse for $\theta \cdot \nabla + \sigma$ with the boundary condition in (1.1). So naturally $-\theta \cdot \nabla + \sigma$ is the associated differential operator for $[T_1^{-1}]^*$.

Thus we can use a first order Euler method to compute $[T_1^{-1}]^*$ just as with T_1^{-1} . Finally, we make note of a formula for $[\chi_V R_+ T_1^{-1}]^* : L^2(\partial_+ S\Omega, d\Sigma) \rightarrow L^2(\Omega \times \mathbb{S}^{n-1})$, which is easily verified to be

$$(4.7) \quad [\chi_V R_+ T_1^{-1}]^*g(x, \theta) = g^\#(x, \theta) \chi_V^\#(x, \theta) E(x, \theta).$$

Recall the truncation parameter $N_{\text{scat}} \in \mathbb{N}$ corresponding to how many terms in the Neumann series $\sum_{m=0}^\infty ([T_1^{-1}]^* K^*)^m$ to use. We proceed as in Algorithm 2.

5. SMOOTHNESS ANALYSIS

When trying to recover microlocally the most singular part of the source via $X_V^* X_V$ as analyzed in [15], it turns out that in theory only the first term of the Neumann series is needed. This is stated in Lemma 2.3, for which we now provide the proof, utilizing the weakly singular integral results in Appendix A.

Algorithm 2 Computing $X_V^* X_V f$

```

1:  $v_0(x, \eta) \leftarrow [\chi_V R_+ T_1^{-1}]^* X_V f(x, \eta) = (X_V f)^\#(x, \eta) E(x, \eta)$ 
2: for  $j = 1$  to  $N_{\text{scat}}$  do
3:    $v_j \leftarrow K_\delta^* v_{j-1}$   $\triangleright$  Apply  $K^*$ 
4:   for  $i = 1$  to  $N_d$  do
5:      $w_{\eta_i}(\mathbf{x}_{N_x}, \mathbf{y}) = 0$   $\triangleright$  Apply  $[T^{-1}]^*$ 
6:     solve  $-\partial_{x_1} w_{\eta_i} + \sigma_{\eta_i} w_{\eta_i} = [v_j]_{\eta_i}$  for  $w_{\eta_i}$ .
7:      $v_j(\mathbf{x}, \mathbf{y}, \eta_i) \leftarrow w = [w_{\eta_i}]_{-\eta_i}(\mathbf{x}, \mathbf{y})$ 
8:   end for
9: end for
10:  $v(\mathbf{x}, \mathbf{y}) \leftarrow \delta \sum_{i=1}^{N_d} \sum_{j=1}^{N_{\text{scat}}} v_j(\mathbf{x}, \mathbf{y}, \eta_i)$   $\triangleright$  Apply  $J^*$ 
11:  $\triangleright v$  is an approximation to  $X_V^* X_V f$ 

```

Proof of Lemma 2.3. Observe that

$$\begin{aligned}
X_V^* &= [\chi_V R_+ T_1^{-1} (\text{Id} - K T_1^{-1})^{-1} J]^* \\
&= \sum_{j=0}^{m_2} [\chi_V R_+ T_1^{-1} (K T_1^{-1})^j J]^* + [\chi_V R_+ T_1^{-1} (K T_1^{-1})^{m_2+1} (\text{Id} - K T_1^{-1})^{-1} J]^* \\
X_V &= \chi_V R_+ T_1^{-1} (\text{Id} - K T_1^{-1})^{-1} J \\
&= \sum_{i=0}^{m_1} \chi_V R_+ T_1^{-1} (K T_1^{-1})^i J + \chi_V R_+ T_1^{-1} (K T_1^{-1})^{m_1+1} (\text{Id} - K T_1^{-1})^{-1} J.
\end{aligned}$$

Thus

$$\begin{aligned}
X_V^* X_V f &= \sum_{j=0}^{m_2} \sum_{i=0}^{m_1} [\chi_V R_+ T_1^{-1} (K T_1^{-1})^j J]^* \chi_V R_+ T_1^{-1} (K T_1^{-1})^i J f \\
&= \sum_{i=0}^{m_1} [\chi_V R_+ T_1^{-1} (\text{Id} - K T_1^{-1})^{-1} (K T_1^{-1})^{m_2+1} J]^* \chi_V R_+ T_1^{-1} (K T_1^{-1})^i J f \\
&+ \sum_{j=0}^{m_2} [\chi_V R_+ T_1^{-1} (K T_1^{-1})^j J]^* \chi_V R_+ T_1^{-1} (K T_1^{-1})^{m_1+1} (\text{Id} - K T_1^{-1})^{-1} J f \\
&+ [\chi_V R_+ T_1^{-1} (\text{Id} - K T_1^{-1})^{-1} (K T_1^{-1})^{m_2+1} J]^* \chi_V R_+ T_1^{-1} (K T_1^{-1})^{m_1+1} (\text{Id} - K T_1^{-1})^{-1} J f \\
&=: A_1 + A_2 + A_3.
\end{aligned}$$

First note that

$$[\chi_V R_+ T_1^{-1}]^* \chi_V R_+ T_1^{-1} f(x, \theta) = \chi_V(x, \theta)^2 \int \exp\left(-\int_s^\infty \sigma(x + \tau\theta, \theta) d\tau\right) f(x + s\theta, \theta) ds.$$

In particular, $[\chi_V R_+ T_1^{-1}]^* \chi_V R_+ T_1^{-1}$ is bounded on $H^j(\Omega \times \mathbb{S}^{n-1})$ for all j . Moreover, from the proof of Proposition 6.1 of [15] we have that $[(\text{Id} - K T_1^{-1})^{-1}]^*$ can be taken to be bounded on $H^j(\Omega \times \mathbb{S}^{n-1})$ whenever $(\text{Id} - K T_1^{-1})^{-1}$ is, which we can assume is the case for $j \leq l + \max\{m_1, m_2\} + 1$.

From the discussion in Appendix A, we have that

$$[(KT_1^{-1})^{m_2+1}J]^*g(x) = \int \int \frac{\beta_{m_2+1}(y, x, |y-x|, \widehat{y-x}, \theta)}{|y-x|^{n-m}} g(y, \theta) dy d\theta.$$

Using a similar argument as in Lemma 2 of [29] and applying Proposition A.1, we have that $[(KT_1^{-1})^{m_2+1}J]^*$ is bounded from $H^l(\Omega \times \mathbb{S}^{n-1}) \rightarrow H^{l+m_2+1}(\Omega \times \mathbb{S}^{n-1})$.

Now, to analyze A_1 we write

$$A_1 = [(KT_1^{-1})^{m_2+1}J]^*[(\text{Id} - KT_1^{-1})^{-1}]^*[\chi_V R_+ T_1^{-1}]^* \chi_V R_+ T_1^{-1} \sum_{i=0}^{m_1} (KT_1^{-1})^i J,$$

and from the arguments of the previous paragraph it is clear that A_1 maps $H^l(\Omega)$ to $H^{l+m_2+1}(\Omega_1)$. Likewise,

$$A_2 = \sum_{j=0}^{m_2} [KT_1^{-1}]^j J^* [\chi_V R_+ T_1^{-1}]^* \chi_V R_+ T_1^{-1} (\text{Id} - KT_1^{-1})^{-1} (KT_1^{-1})^{m_1+1} J$$

and so A_2 maps $H^l(\Omega)$ to $H^{l+m_1+1}(\Omega_1)$. A similar argument shows that A_3 maps $H^l(\Omega)$ to $H^{l+m_1+m_2+2}(\Omega_1)$. \square

6. NUMERICAL COMPUTATIONS

For our numerical computations, the goal is to provide visual verification of Theorem 2.1, and more specifically, of the related result of Lemma 2.3. In all examples, we use a cartesian grid of 256 by 256 with 128 directions θ . We'll use the notation (x, y) to denote a point in \mathbb{R}^2 . In order to incorporate anisotropy in k , we use the Henyey-Greenstein (H-G) phase function [14], which is very commonly used in optical imaging:

$$(6.1) \quad p(\theta, \theta') = \begin{cases} \frac{1}{2\pi} \frac{1-g^2}{1+g^2-2g\theta \cdot \theta'} & n=2, \\ \frac{1}{4\pi} \frac{1-g^2}{(1+g^2-2g\theta \cdot \theta')^{3/2}} & n=3. \end{cases}$$

To set $g=0$ corresponds to the isotropic case, while $g=1$ and $g=-1$ correspond to forward scattering and backscattering, respectively. In typical applications g is around 0.80 to 0.95 ([12]), which is characteristic of highly forward-peaked scattering.

We also incorporate noise into the boundary data in the following way. The noiseless data Xf is an $m \times 128$ matrix, with the rows corresponding to the position along the unit circle and the columns corresponding to the particles' direction. Given a parameter $\mu > 0$, for the j th column v_j of Xf (i.e. $[Xf]_j$) we compute $\|v_j\|_2 = \sqrt{v_j^T v_j}$ and generate a vector w of length m with values chosen randomly according to the standard normal distribution (variance 1 and mean 0). We then define the j th column of the noisy data by

$$(6.2) \quad [Xf_{\text{noise}}]_j := [Xf]_j + \mu \sqrt{[Xf]_j^T [Xf]_j} \frac{w}{\sqrt{w^T w}} = v_j + \mu \|v_j\|_2 \frac{w}{\|w\|_2}.$$

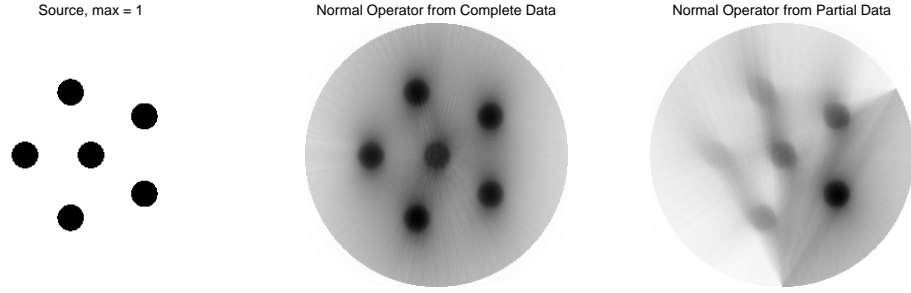


FIGURE 3. A source consisting of circular bump functions with height 1. The partial data is measured without noise on the set $V = V_{\text{examples}}$.

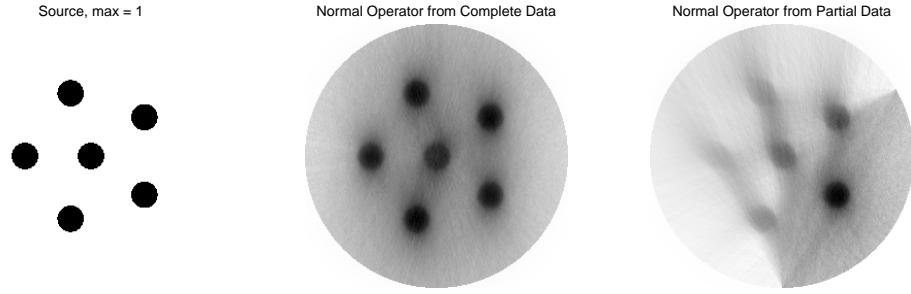


FIGURE 4. Same as Figure 3 except with a noise coefficient $\mu = 0.50$.

Thus μ represents the fraction of $\|v_j\|_2$ to which we would like to rescale the variance of the noise.

With these details in mind, for all computed examples we have taken

$$k(x, y, \theta, \theta') = \frac{1}{2\pi} \chi_{\{x^2+y^2 < 1\}}(x, y) (0.05 + \sin^2 xy) \frac{1 - 0.85^2}{1 + 0.85^2 - 2 \cdot 0.85 \cdot \theta \cdot \theta'}$$

and

$$\sigma(x, y, \theta) = 0.5 \chi_{\{x^2+y^2 < 1\}}(x, y) [0.05 + \cos^2 xy] \sin^2 \theta.$$

Moreover, using the notation of Lemma 2.3, we take $m_1 = 8$ and $m_2 = 2$. This corresponds to computing the first 9 terms of the Neumann series expansion for Xf and only 3 terms in the series representation of X^* . Finally, in all computations we take

$$(6.3) \quad V = V_{\text{examples}} = (\eta, \theta) \in \partial_+ S\Omega = \partial\mathbb{D} \times \mathbb{S}^1 \mid \eta \in [0, \pi/3] \text{ and } \eta \cdot \theta > 0\}.$$

7. CONCLUSIONS

We have presented a numerical method to solve the direct problem for the Radiative Transfer Equation (1.1) based on the work of [19], which utilizes the discrete Fourier transform and fractional discrete Fourier transform to

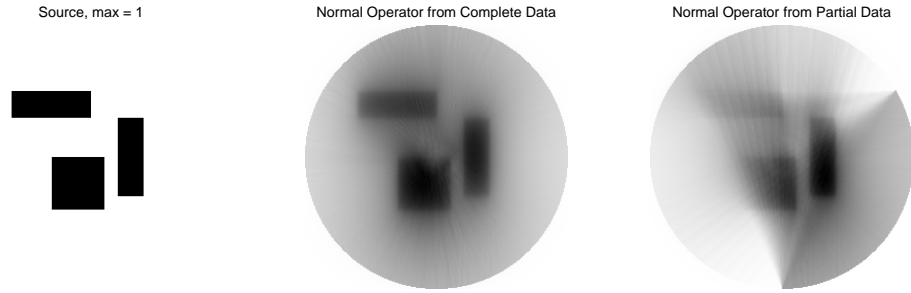


FIGURE 5. A source consisting of rectangular bump functions with height 1. The partial data is measured without added noise on the same set V as given in Figure 3.

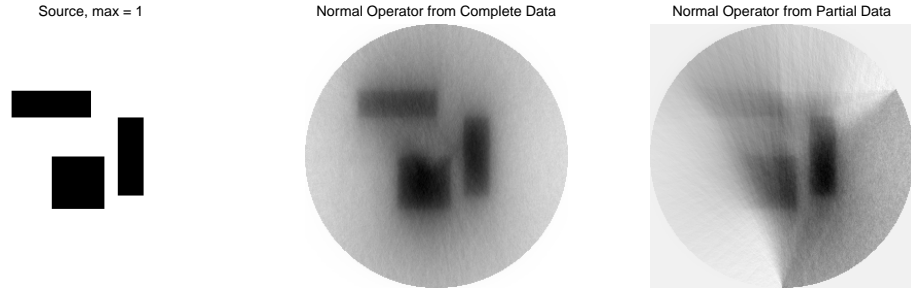


FIGURE 6. Same as Figure 5 except with a noise coefficient $\mu = 0.5$.

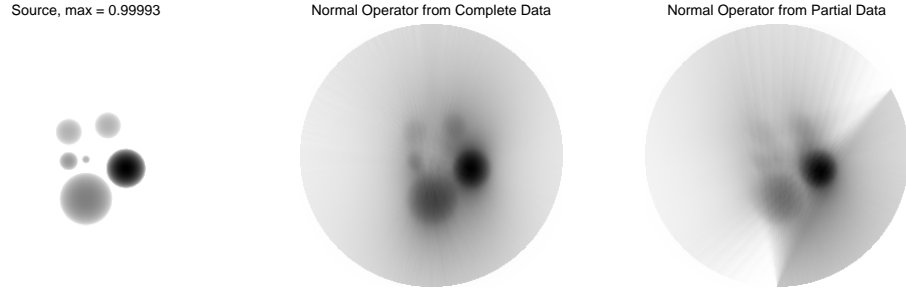


FIGURE 7. A spiral pattern of continuous circular bump functions of the form $g(x, y) = A\sqrt{1 - \frac{1}{r^2}(x - x_0)^2 - \frac{1}{r_0^2}(y - y_0)^2}$, where A is the maximum height and r is the radius. In this example, starting from the largest bump and moving counterclockwise, we have the set of heights and radii $A = \{0.5, 1, 0.3, 0.3, 0.4, 0.3\}$ and $r = \{0.2, 0.15, 0.1, 0.1, 0.07, 0.03\}$, respectively. The partial data is measured with no added noise on the set V given in Figure 3.

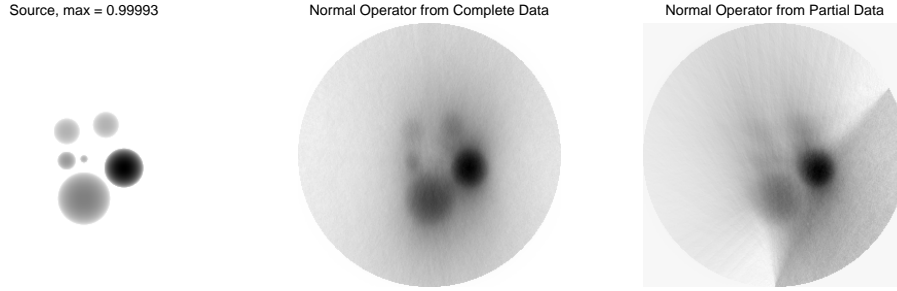


FIGURE 8. Same as Figure 7, but with an added noise coefficient $\mu = 0.50$.

implement a rotation-based method for computing the necessary line integrals. Moreover, we have computed the normal operator $X_V^* X_V$ in a similar manner, where X_V is the partial data operator. Ultimately, this has given us some nice visual examples in the presence of anisotropic (σ, k) with or without added noise, where the anisotropic parts of the parameters have physically meaningful structure as given in [12, 14]. Such examples visually demonstrate the ability to detect the singularities of an unknown source with only partial data of the transport solution u at the boundary.

Most importantly, the results of Figures 3 through 8 show the detection of edges resulting from singularities in the respective chosen sources f , and this is consistent with what is theoretically predicted in Theorem 2.1 and with the microlocally visible set \mathcal{M}' given in (2.3). Moreover, it provides a nice generalization of similar well-known results regarding the detectable singularities in the context of limited data computed X-ray tomography, see [23].

Acknowledgements. This research was supported by NSF grant DMS-0838212. The author wishes to thank Francois Monard for some helpful conversations related to the computational aspects of this work. Much of the work in Appendix A was completed during a visit to Finland under the advisement of Mikko Salo, with whom it was very informative to talk about this and related problems.

APPENDIX A. SMOOTHING PROPERTIES OF COMPOSITIONS OF WEAKLY SINGULAR-TYPE INTEGRAL OPERATORS

Let's consider an operator of type

$$[Af](x, \theta) = \int \frac{\alpha(x, y, |x - y|, \widehat{x - y}, \theta)}{|x - y|^{n-1}} f(y, \widehat{x - y}) dy$$

where $\alpha(x, y, r, \eta, \theta) \in C_c^\infty(\mathbb{R}^n \times \mathbb{R}^n \times \mathbb{R}_+ \times \mathbb{S}^{n-1} \times \mathbb{S}^{n-1})$. We would like to analyze compositions of the form $[A^m Jf](x, \theta)$ where $J : L^2(\mathbb{R}^n) \rightarrow L^2(\mathbb{R}^n \times \mathbb{S}^{n-1})$ is the extension operator $Jf(x, \theta) = f(x)$ as used previously.

For $m = 2$, we compute

$$\begin{aligned}
& [A^2 Jf](x, \theta) \\
&= \int \frac{\alpha(x, y_1, |x - y_1|, \widehat{x - y_1}, \theta)}{|x - y_1|^{n-1}} [AJf] \left(y_1, \frac{x - y_1}{|x - y_1|} \right) dy_1 \\
&= \int \frac{\alpha(x, y_1, |x - y_1|, \widehat{x - y_1}, \theta)}{|x - y_1|^{n-1}} \int \frac{\alpha \left(y_1, y_2, |y_1 - y_2|, \widehat{y_1 - y_2}, \widehat{x - y_1} \right)}{|y_1 - y_2|^{n-1}} f(y_2) dy_2 dy_1 \\
&= \int \left[\int \frac{\alpha(x, y_1, |x - y_1|, \widehat{x - y_1}, \theta) \alpha \left(y_1, y_2, |y_1 - y_2|, \widehat{y_1 - y_2}, \widehat{x - y_1} \right)}{|x - y_1|^{n-1} |y_1 - y_2|^{n-1}} dy_1 \right] f(y_2) dy_2.
\end{aligned}$$

Similarly for $m = 3$,

$$\begin{aligned}
& [A^3 Jf](x, \theta) \\
&= \int \left(\int \int \frac{\alpha(x, y_1, |x - y_1|, \widehat{x - y_1}, \theta) \alpha \left(y_1, y_2, |y_1 - y_2|, \widehat{y_1 - y_2}, \widehat{x - y_1} \right)}{|x - y_1|^{n-1} |y_1 - y_2|^{n-1} |y_2 - y_3|^{n-1}} \right. \\
&\quad \left. \cdot \alpha \left(y_2, y_3, |y_2 - y_3|, \widehat{y_2 - y_3}, \widehat{y_1 - y_2} \right) dy_2 dy_1 \right) f(y_3) dy_3
\end{aligned}$$

In general, define

$$\begin{aligned}
& \alpha_1 := \alpha, \\
& \alpha_2(x, y_1, y_2, |x - y_1|, |y_1 - y_2|, \widehat{x - y_1}, \widehat{y_1 - y_2}, \theta) := \alpha_1(x, y_1, |x - y_1|, \widehat{x - y_1}, \theta) \\
&\quad \cdot \alpha_1 \left(y_1, y_2, |y_1 - y_2|, \widehat{y_1 - y_2}, \widehat{x - y_1} \right), \\
& \text{(A.1)} \\
& \alpha_m(x, y_1, \dots, y_m, |x - y_1|, \dots, |y_{m-1} - y_m|, \widehat{x - y_1}, \dots, \widehat{y_{m-1} - y_m}, \theta) := \\
&\quad \alpha_{m-1}(y_1, y_2, \dots, y_m, |y_1 - y_2|, \dots, |y_{m-1} - y_m|, \widehat{y_1 - y_2}, \dots, \widehat{y_{m-1} - y_m}, \widehat{x - y_1}) \\
&\quad \cdot \alpha_1(x, y_1, |x - y_1|, \widehat{x - y_1}, \theta),
\end{aligned}$$

where $y_0 := x$. For simplicity of notation, define

$$\begin{aligned}
\mathbf{y}_m &:= (y_1, \dots, y_{m-1}, y) \\
r_m &:= (|y_1 - y_2|, \dots, |y_{m-1} - y|) \\
\widehat{\mathbf{r}}_m &:= (\widehat{y_1 - y_2}, \dots, \widehat{y_{m-1} - y}).
\end{aligned}$$

Then set for $m \geq 2$

$$a_m(x, y, \theta) := \int \dots \int \frac{\alpha_m(x, \mathbf{y}_m, |x - y_1|, r_m, \widehat{x - y_1}, \widehat{\mathbf{r}}_m, \theta)}{|x - y_1|^{n-1} |y_1 - y_2|^{n-1} \dots |y_{m-1} - y|^{n-1}} dy_1 \dots dy_{m-1}.$$

Also let

$$a_0 := J[\delta(\cdot - y)], \quad a_1(x, y, \theta) := \frac{\alpha_1(x, y, |x - y|, \widehat{x - y}, \theta)}{|x - y|^{n-1}}.$$

Then

$$[A^m Jf](x, \theta) = \int a_m(x, y, \theta) f(y) dy, \quad m \geq 0.$$

Now we would like to show that $A^m J$ has a kernel of the form

$$(A.2) \quad \frac{\beta_m(x, y, |x - y|, \widehat{x - y}, \theta)}{|x - y|^{n-m}}$$

where $\beta_m(x, y, r, \eta, \theta)$ is C^∞ . Ultimately, our goal is to rigorously show for $m \geq 2$ that $A^m J$ is a pseudodifferential operator of order $-m$, by adapting the proof of Lemma 2 in [11], which already directly applies to the case $m = 1$.

A.1. The Case $m = 2$. For $\eta \in \mathbb{S}^{n-1}$, define the set $\mathcal{D}_\eta := \mathbb{R}^n \setminus (B_0(1/4) \cup B_\eta(1/4))$. Also let A_η be the rotational matrix such that $A_\eta \eta = e_1$, the first unit basis vector of \mathbb{R}^n . Let $\psi(r)$ be a smooth, even bump function such that $0 \leq \psi \leq 1$, $\psi \equiv 1$ for $|r| \leq 1/4$, and $\psi \equiv 0$ for $|r| \geq 1/2$. We will frequently use the notation $r = |x - y|$ and $\eta = \widehat{x - y}$. Note that differentiation of A_η with respect to x yields, from the fact that $\partial_{x_j} \widehat{x - y} = \frac{x_j - y_j}{|x - y|^2}$, that $|\partial_{x_j} A_\eta| \leq \frac{C}{|x - y|}$. Similarly, l th order derivatives of A_η with respect to x will have bounds of the form $\frac{C}{|x - y|^l}$. Of course, if we treat A_η as a matrix of functions of η only, and not implicitly dependent on x , then each such coordinate function is in $C^\infty(\mathbb{S}^{n-1})$.

We have

$$a_2(x, y, \theta) = \int \frac{\alpha_2(x, y_1, y, |x - y_1|, |y_1 - y|, \widehat{x - y_1}, \widehat{y_1 - y}, \theta)}{|x - y_1|^{n-1} |y_1 - y|^{n-1}} dy_1.$$

We may then cut up the above integral, using ψ and suppressing some variables, to obtain

$$\begin{aligned} & \int \psi \left(\frac{|x - y_1|}{|x - y|} \right) \alpha_2 dy_1 + \int \psi \left(\frac{|y_1 - y|}{|x - y|} \right) \alpha_2 dy_1 \\ & + \int \left[1 - \psi \left(\frac{|x - y_1|}{|x - y|} \right) - \psi \left(\frac{|y_1 - y|}{|x - y|} \right) \right] \alpha_2 dy_1 \\ & =: I_1 + I_2 + I_3. \end{aligned}$$

Let's focus on the first term. Substitute $w = \frac{x - y_1}{|x - y|}$ so that $|x - y|^n dw = dy_1$, $y_1 = x - |x - y|w$ and $y_1 - y = |x - y|(\widehat{x - y} - w)$. We also note that the

region of integration is $w \in B_0(\frac{1}{2})$. We obtain

$$\begin{aligned}
I_1 &= \int \frac{\psi\left(\frac{|x-y_1|}{|x-y|}\right) \alpha_2(x, y_1, y, |x-y_1|, |y_1-y|, \widehat{x-y_1}, \widehat{y_1-y}, \theta)}{|x-y_1|^{n-1} |y_1-y|^{n-1}} dy_1 \\
&= \frac{1}{|x-y|^{n-2}} \int \frac{\psi(|w|)}{|w|^{n-1} |\widehat{x-y-w}|^{n-1}} \\
&\quad \cdot \alpha_2\left(x, x-|x-y|w, y, |x-y||w|, |x-y||\widehat{x-y-w}|, \widehat{w}, \frac{\widehat{x-y-w}}{|\widehat{x-y-w}|}, \theta\right) dw \\
&= \frac{1}{r^{n-2}} \int_{B_0(1/2)} \frac{\psi(|w|) \alpha_2\left(x, x-|x-y|w, y, |x-y||w|, |x-y||\eta-w|, \widehat{w}, \widehat{\eta-w}, \theta\right)}{|w|^{n-1} |\eta-w|^{n-1}} dw \\
&= \frac{1}{r^{n-2}} \int_{B_0(1/2)} \frac{\psi(|w|) \alpha_2\left(x, x-rA_\eta^{-1}w, y, r|w|, r|e_1-w|, \widehat{w}, A_\eta^{-1}\widehat{e_1-w}, \theta\right)}{|w|^{n-1} |e_1-w|^{n-1}} dw.
\end{aligned}$$

Let's consider the other terms:

$$\begin{aligned}
I_2 &= \int \frac{\psi\left(\frac{|y_1-y|}{|x-y|}\right) \alpha_2(x, y_1, y, |x-y_1|, |y_1-y|, \widehat{x-y_1}, \widehat{y_1-y}, \theta)}{|x-y_1|^{n-1} |y_1-y|^{n-1}} dy_1 \\
&= \frac{1}{r^{n-2}} \int_{B_0(1/2)} \frac{\psi(|\widehat{x-y-w}|) \alpha_2\left(x, x-rA_\eta^{-1}w, y, r|w|, r|e_1-w|, \widehat{w}, A_\eta^{-1}\widehat{e_1-w}, \theta\right)}{|w|^{n-1} |e_1-w|^{n-1}} dw \\
I_3 &= \int \frac{\left(1 - \psi\left(\frac{|x-y_1|}{|x-y|}\right) - \psi\left(\frac{|y_1-y|}{|x-y|}\right)\right) \alpha_2(x, y_1, y, |x-y_1|, |y_1-y|, \widehat{x-y_1}, \widehat{y_1-y}, \theta)}{|x-y_1|^{n-1} |y_1-y|^{n-1}} dy_1 \\
&= \frac{1}{r^{n-2}} \int_{\mathcal{D}_{e_1}} \frac{(1 - \psi(|w|) - \psi(|e_1-w|))}{|w|^{n-1} |e_1-w|^{n-1}} \\
&\quad \cdot \alpha_2\left(x, x-rA_\eta^{-1}w, y, r|w|, r|e_1-w|, \widehat{w}, A_\eta^{-1}\widehat{e_1-w}, \theta\right) dw
\end{aligned}$$

Notice that after multiplying each term by r^{n-2} , the remaining integrals are smooth in the variables x, y, r, η and θ .

A.2. The General Case. We seek to record a general formula for the integral representation of $A^m Jf(x)$ which resembles a weakly singular integral with integral singularity $\frac{1}{|x-y|^{n-m}}$. Let's make some new definitions to simplify the notation. Set $y_0 = x$ and $y_m = y_{m+1} = y$, and given $1 \leq j \leq m-1$, define

$$w_j := \frac{x - y_j}{|x - y_{j+1}|}, \quad w'_j := \frac{y_j - y_{j+1}}{|x - y_{j+1}|}.$$

Note that $\eta = \widehat{x - y} = w_m$. Also define $w_0 = 0$ for convenience, and then set

$$\begin{aligned}\psi_j^1(w_j, w'_j) &:= \psi(|w_j|) \\ \psi_j^2(w_j, w'_j) &:= \psi(|w'_j|) \\ \psi_j^3(w_j, w'_j) &:= 1 - \psi(|w_j|) - \psi(|w'_j|).\end{aligned}$$

We notice a few useful formulas for $1 \leq j \leq m-1$

$$\begin{aligned}w'_j &= \widehat{w_{j+1}} - w_j \\ y_j &= x - |x - y| w_j \prod_{l=j+1}^{m-1} |w_l| \\ y_j - y_{j+1} &= |x - y_{j+1}| (\widehat{w_{j+1}} - w_j).\end{aligned}$$

Define

$$\begin{aligned}\mathbf{y} &:= [y_1, \dots, y_{m-1}, y] = \left[\left\{ x - |x - y| w_j \prod_{l=j+1}^{m-1} |w_l| \right\}_{j=1}^{m-1}, y \right] \in \mathbb{R}^m, \\ |\mathbf{w}| &:= \left[\prod_{l=j}^{m-1} |w_l| \right]_{j=1}^{m-1}.\end{aligned}$$

We can partition the integrations involved in $\alpha_m(x, y, \theta)$ as

$$\begin{aligned}& \int \sum_{\gamma \in \{1,2,3\}^m} \left[\prod_{j=1}^{m-1} \psi_j^{\gamma_j}(w_j, \widehat{w_{j+1}} - w_j) \right] \\ & \cdot \frac{\alpha_m(x, \mathbf{y}, r|\mathbf{w}|, \widehat{w_1}, \frac{\widehat{w_2} - w_1}{|\widehat{w_2} - w_1|}, \dots, \frac{\eta - w_{m-1}}{|\eta - w_{m-1}|}, \theta)}{r^{n-m} |\eta - w_{m-1}|^{n-1} \prod_{l=1}^{m-1} |w_l|^{n-l-1} \prod_{k=1}^{m-2} |\widehat{w_{k+1}} - w_k|^{n-1}} dw_1 \dots dw_{m-1}.\end{aligned}$$

For $0 \leq j \leq m-1$ define

$$\begin{aligned}\mathcal{D}_j^1 &:= B_0(1/2) \\ \mathcal{D}_j^2 &:= B_{\widehat{w_{j+1}}}(1/2) \\ \mathcal{D}_j^3 &:= \mathbb{R}^n \setminus (B_0(1/4) \cup B_{\widehat{w_{j+1}}}(1/4)).\end{aligned}$$

Then for each $\gamma \in \{1, 2, 3\}_{j=1}^{m-1}$, set $\mathcal{D}_\gamma := \prod_{j=1}^{m-1} \mathcal{D}_j^{\gamma_j}$. Then we have the integral

$$(A.3) \quad I_m(x, y, r, \eta, \theta) = \sum_{\gamma \in \{1, 2, 3\}^{m-1}} \int_{\mathcal{D}_\gamma} \left[\prod_{j=1}^{m-1} \psi_j^{\gamma_j}(w_j, \widehat{w_{j+1}} - w_j) \right] \cdot \frac{\alpha_m(x, \mathbf{y}, r|\mathbf{w}|, \widehat{w_1}, \frac{\widehat{w_2} - w_1}{|\widehat{w_2} - w_1|}, \dots, \frac{\eta - w_{m-1}}{|\eta - w_{m-1}|}, \theta)}{r^{n-m} |\eta - w_{m-1}|^{n-1} \prod_{l=1}^{m-1} |w_l|^{n-l-1} \prod_{k=1}^{m-2} |\widehat{w_{k+1}} - w_k|^{n-1}} dw_1 \dots dw_{m-1}.$$

We then define

$$(A.4) \quad \beta_m(x, y, r, \eta, \theta) := r^{n-m} I_m(x, y, r, \eta, \theta),$$

so that

$$A^m Jf(x) = \int \frac{\beta_m(x, y, |x - y|, \widehat{x - y}, \theta)}{|x - y|^{n-m}} f(y) dy.$$

In order to justify the convergence of such an iterated integral (as we have changed the order around), we first note that x and y are restricted to Ω by assumption. Secondly, the singularities in each variable w_j are all locally integrable since near such singularities we have local behavior like $\frac{1}{|w_j|^{n-j-1}}$ or $\frac{1}{|\widehat{w_{j+1}} - w_j|^{n-1}}$. It remains to show bounds on the terms in the sum which involve integrations over one or more of the domains $\mathcal{D}_j^3 := \mathbb{R}^n \setminus (B_0(1/4) \cup B_{\widehat{w_{j+1}}}(1/4))$. Let j be the first such index where such an integration occurs in a given term. We may integrate out the variables $w_1 \dots w_{j-1}$ first since the domains of integration are bounded in those cases. Since $y_j \in \Omega$, we have $x - rw_j \prod_{l=j+1}^{m-1} |w_l| \in \Omega$. Thus

$$|w_j| \leq \frac{\text{diam}(\Omega)}{r \prod_{l=j+1}^{m-1} |w_l|} =: M.$$

So we may estimate the integral by

$$\begin{aligned} & \int_{\mathcal{D}_\gamma} \frac{C}{r^{n-m} |\eta - w_{m-1}|^{n-1} |\widehat{w_{m-1}} - w_{m-2}|^{n-1} \dots |\widehat{w_{j+2}} - w_{j+1}|^{n-1}} \\ & \cdot \frac{1}{\prod_{l=j+1}^{m-1} |w_l|^{n-l-1}} \left[\frac{1}{u^{n-j-2}} \right]_1^M dw_{j+1} \dots dw_{m-1} \\ & \leq \frac{\text{diam}(\Omega)^{2+j-n}}{r^{j+2-m}} \int_{\mathcal{D}'_\gamma} \frac{C}{|\eta - w_{m-1}|^{n-1} |\widehat{w_{m-1}} - w_{m-2}|^{n-1} \dots |\widehat{w_{j+2}} - w_{j+1}|^{n-1}} \\ & \cdot \frac{1}{\prod_{l=j+1}^{m-1} |w_l|^{j+1-l}} dw_{j+1} \dots dw_{m-1}, \end{aligned}$$

where \mathcal{D}'_γ is the domain obtained from \mathcal{D}_γ by removing the domains of integration with respect to $w_1 \dots w_j$. Since $1 \leq j \leq m-1$, we have that $3-m \leq 2+j-m \leq 1$. In all cases, the behavior in r is an integrable

singularity since $n \geq 2$. Further integrations over domains \mathcal{D}_j^3 will result in similar estimates, and in all cases the power on r remains integrable. It follows that, upon multiplying the whole integral by r^{n-1} , we obtain a function that is C^∞ in x, y, r and θ , since the multiplicative factor of r has exponent between $n-2$ and $n+m-3$, all of which are smooth at 0.

It remains to show smoothness in η . Notice that when $\gamma_{m-1} = 1$ or 3 (i.e. when $w_{m-1} \in B_0(1/2)$ or $w_{m-1} \in \mathbb{R}^n \setminus (B_0(1/4) \cup B_\eta(1/4))$), then $|\eta - w_{m-1}|$ is uniformly positive. Thus, we can differentiate under the integral sign with respect to η the term $\frac{1}{|\eta - w_{m-1}|^{n-1}}$ infinitely many times. On the other hand, to differentiate the terms with $\gamma_{m-1} = 2$ (i.e. $w_{m-1} \in B_\eta(1/2)$), we make the substitution $z_{m-1} = \eta - w_{m-1}$ and note that $z_{m-1} \in B_0(1/2)$. Then term $\frac{1}{|w_{m-1}|^{n-m}} = \frac{1}{|\eta - z_{m-1}|^{n-m}}$ is uniformly bounded away from 0, so we may differentiate it arbitrarily many times with respect to η . The only other potential problem will occur if in addition, $\gamma_{m-2} = 2$ or equivalently, $w_{m-2} \in \widehat{B_{w_{m-1}}}(1/2) = \widehat{B_{\eta - z_{m-1}}}(1/2)$. In this case, we make yet another change of variables $z_{m-2} = \widehat{w_{m-1}} - w_{m-2} = \widehat{\eta - z_{m-1}} - w_{m-2}$, so that $z_{m-2} \in B_0(1/2)$ and the term $\frac{1}{|\widehat{w_{m-1}} - w_{m-2}|^{n-1}}$ does not depend on η . Similarly, the term $\frac{1}{|w_{m-2}|^{n-m+1}} = \frac{1}{|\widehat{\eta - z_{m-1}} - z_{m-2}|^{n-m+1}}$ is uniformly bounded for $z_{m-2} \in B_0(1/2)$, and so we can differentiate it arbitrarily many times with respect to η . Continuing in this way, if at any point $\gamma_j = 2$ we make the change of variables $z_j = \widehat{w_{j+1}} - w_j$ and obtain similar bounds. The main idea is to transfer the derivative to the numerator function α_m . It is a routine matter to check that under such change of variables, differentiation of α_m with respect to η does not result in any unbounded factors involving η via the chain rule.

Remark 1. By the same reasoning, if $\alpha(x, y, r, \eta, \theta)$ is in $C_c^2(\mathbb{R}^n \times \mathbb{R}^n \times \mathbb{R}_+ \times \mathbb{S}^{n-1} \times \mathbb{S}^{n-1})$, then $\beta_m \in C_c^2$.

We now consider the following adaptation of Lemma 2 from [11]:

Lemma A.1. *Let $m \geq 1$ and let $\mathcal{A} : C_0(\Omega) \rightarrow C(\Omega, \mathbb{S}^{n-1})$ be the operator*

$$\mathcal{A}f(x, \theta) = \int_{\mathbb{S}^{n-1}} \int_{\mathbb{R}} r^{m-1} \alpha(x, r, \omega, \theta) f(x + r\omega) dr d\omega,$$

where $\alpha \in C^\infty(\Omega \times \mathbb{R} \times \mathbb{S}^{n-1} \times \mathbb{S}^{n-1})$. Then \mathcal{A} is a classical ΨDO of order $-m$ with full symbol

$$a(x, \xi) \sim \sum_{k=m-1}^{\infty} a_k(x, \xi),$$

where

$$a_k(x, \xi) = 2\pi \frac{i^k}{k!} \int_{\mathbb{S}^{n-1}} \partial_r^k A(x, 0, \omega, \theta) \delta^{(k)}(\omega \cdot \xi) d\omega.$$

Proof. The proof directly follows from the proof of the case $m = 1$ in [11]. Let $A'(x, r, \omega, \theta) = r^{m-1}A(x, r, \omega, \theta)$, and note that if A' is an odd function of (r, ω) , then $\mathcal{A}f = 0$. So we may replace $A' = r^{m-1}A$ by

$$\begin{aligned} A'_{\text{even}}(r, \omega) &= \frac{1}{2}(A'(r, \omega) + A'(-r, -\omega)) \\ &= \frac{1}{2}(r^{m-1}A(r, \omega) + (-r)^{m-1}A(-r, -\omega)) \\ &= \frac{r^{m-1}}{2}(A(r, \omega) + (-1)^{m-1}A(-r, -\omega)). \end{aligned}$$

We can then integrate over $r \geq 0$ only and double the result. Thus,

$$\mathcal{A}f(x) = 2 \int_{\mathbb{S}^{n-1}} \int_0^\infty A'_{\text{even}}(x, r, \omega, \theta) f(x + r\omega) dr d\omega.$$

Changing to polar coordinates via $z = r\omega$ and setting $y = x + r\omega$, we obtain

$$\mathcal{A}f(x) = 2 \int A'_{\text{even}} \left(x, |y - x|, \frac{y - x}{|y - x|}, \theta \right) \frac{f(y)}{|y - x|^{n-1}} dy.$$

We then use a finite Taylor expansion of $A'_{\text{even}}(x, r, \omega, \theta)$ in r near $r = 0$ with $N > 0$ to get

$$A'_{\text{even}}(x, r, \omega, \theta) = \sum_{k=0}^{N-1} A'_{\text{even},k}(x, \omega, \theta) r^k + r^N R_N(x, r, \omega, \theta).$$

One can compute that $2A'_{\text{even},k}(x, \omega, \theta) = A'_k(x, \omega, \theta) + (-1)^k A'_k(x, -\omega, \theta)$, where $k!A'_k = \partial_r^k|_{r=0}A' = \partial_r^k|_{r=0}[r^{m-1}A]$. Clearly, $A'_k = 0$ for all $k < m-1$. Therefore, following the proof of Lemma 2 in [11], we obtain that the terms $a_k(x, \xi, \theta) = 2\pi i^k \int_{\mathbb{S}^{n-1}} A'_k(x, \omega, \theta) \delta^{(k)}(\omega \cdot \xi) d\omega = 0$ for all $k < m-1$. \square

Proposition A.1. *Let $\alpha \in C_c^\infty(\mathbb{R}^n \times \mathbb{R}^n \times \mathbb{R} \times \mathbb{S}^{n-1} \times \mathbb{S}^{n-1})$ and consider the operator $A : L^2(\mathbb{R}^n \times \mathbb{S}^{n-1}) \rightarrow L^2(\mathbb{R}^n; C^\infty(\mathbb{S}^{n-1}))$ defined by*

$$[Af](x, \theta) = \int \frac{\alpha(x, y, |x - y|, \widehat{x - y}, \theta)}{|x - y|^{n-1}} f(y, \widehat{x - y}) dy.$$

Then for $m \geq 1$, $A^m J$ is a classical pseudodifferential operator of order $-m$ with smooth parameter θ , where $J : L^2(\mathbb{R}^n) \rightarrow L^2(\mathbb{R}^n \times \mathbb{S}^{n-1})$ is the extension operator $Jf(x, \theta) = f(x)$.

Proof. Recall that

$$\begin{aligned}
 [A^m J f](x, \theta) &= \int I_m(x, y, |x - y|, \widehat{x - y}, \theta) f(y) dy \\
 &= \int \frac{\beta_m(x, y, |x - y|, \widehat{x - y}, \theta)}{|x - y|^{n-m}} f(y) dy \\
 &= \int_{\mathbb{S}^{n-1}} \int_0^\infty r^{m-1} \beta_m(x, x - r\omega, r, \omega, \theta) f(x - r\omega) dr d\omega \\
 &= \int_{\mathbb{S}^{n-1}} \int_0^\infty r^{m-1} \beta_m(x, x + r\omega, r, -\omega, \theta) f(x + r\omega) dr d\omega.
 \end{aligned}$$

We can then apply Lemma A.1 to complete proof. \square

Let us also compute the adjoint of the operator $A^m J$. Given functions $f \in L^2(\mathbb{R}^n \times \mathbb{S}^{n-1})$ and $g \in L^2(\mathbb{R}^n)$, we have

$$\begin{aligned}
 \langle [A^m J]^* f, g \rangle_{L^2(\mathbb{R}^n)} &= \langle f, A^m J g \rangle_{L^2(\mathbb{R}^n \times \mathbb{S}^{n-1})} \\
 &= \int \int \int \frac{\beta_m(x, y, |x - y|, \widehat{x - y}, \theta)}{|x - y|^{n-m}} g(y) f(x, \theta) dy dx d\theta \\
 &= \int g(y) \left(\int_{\mathbb{R}^n} \int_{\mathbb{S}^{n-1}} \frac{\beta_m(x, y, |x - y|, \widehat{x - y}, \theta)}{|x - y|^{n-m}} f(x, \theta) dx d\theta \right) dy.
 \end{aligned}$$

Thus

$$[A^m J]^* f(x) = \int_{\mathbb{R}^n} \int_{\mathbb{S}^{n-1}} \frac{\beta_m(y, x, |y - x|, \widehat{y - x}, \theta)}{|x - y|^{n-m}} f(y, \theta) d\theta dy.$$

It is then clear that $[A^m J]^* : H^l(\Omega \times \mathbb{S}^{n-1}) \rightarrow H^{l+m}(\Omega)$ using a similar argument as in Lemma 2 of [29] together with Proposition A.1.

REFERENCES

- [1] S. R. Arridge. Optical tomography in medical imaging. *Inverse Problems*, 15:R41–R93, 1999.
- [2] D.H. Bailey and P.N. Swartztrauber. The fractional Fourier transform and applications. *SIAM Rev*, 33:389–404, 1991.
- [3] G. Bal. Inverse transport theory and applications. *Inverse Problems*, 25(055006), 2009.
- [4] G. Bal and A. Tamasan. Inverse source problems in transport equations. *SIAM J. Math. Anal.*, 39(1):57–76, 2007.
- [5] J. Boman and J.O. Strömberg. Novikov’s inversion formula for the attenuated radon transform - a new approach. *The Journal of Geometric Analysis*, 14(2), 2004.
- [6] J. Chang, L. Barbour, and H. Graber. Imaging of fluorescence in highly scattering media. *em IEEE Trans. Biomed. Eng.*, 44(9):810–822, 1997.
- [7] M. Choulli and P. Stefanov. Inverse scattering and inverse boundary value problems for the linear Boltzmann equation. *Comm. Partial Differential Equation*, 21(5-6):763–785, 1996.
- [8] M. Choulli and P. Stefanov. An inverse boundary value problem for the stationary transport equation. *Osaka J. Math.*, 36(1):87–104, 1998.

- [9] P.R. Contag, I.N. Olomu, D.K. Stevenson, and C.H. Contag. Bioluminescent indicators in living mammals. *Nature Medicine*, 4(2):245–247, 1998.
- [10] Robert Dautray and Jacques-Louis Lions. *Mathematical Analysis and Numerical Methods for Science and Technology*, volume 6. Springer-Verlag, 1985.
- [11] B. Frigyik, P. Stefanov, and G. Uhlmann. The x-ray transform for a generic family of curves and weights. *J. Geom. Anal.*, 18(1):81–97, 2008.
- [12] Hao Gao and Hongkai Zhao. A fast forward solver of radiative transfer equation. *Trans. Th. Stat. Phys.*, 38:149–192, 2009.
- [13] A. Grigis and J. Sjöstrand. *Microlocal Analysis for Differential Operators: An Introduction*, volume 196 of *London Mathematical Society Lecture Note Series*. Cambridge University Press, New York, 1994.
- [14] L.G. Henyey and J.L. Greenstein. Diffuse radiation in the galaxy. *Astrophys. J.*, 93:70–83.
- [15] M. Hubenthal. An inverse source problem in radiative transfer with partial data. *Inverse Problems*, 27(125009), 2011.
- [16] H.B. Jiang, S. Ramesh, and M. Barlett. Combined optical and fluorescence imaging for breast cancer detection and diagnosis. *Crit. Rev. Biom. Eng.*, 28(3-4):371–375, 2000.
- [17] E.W. Larsen. The inverse source problem in radiative transfer. *J. Quant. Spect. Radiat. Transfer*, 15, 1975.
- [18] S.G. Mikhlin and S. Prössdorf. *Singular Integral Operators*. Springer-Verlag, Berlin, 1986. Translated from the German by Albrecht Böttcher and Reinhard Lehmann.
- [19] F. Monard and G. Bal. An accurate solve for forward and inverse transport. *Journal of Computational Physics*, 229(13), July 2010.
- [20] R.G. Novikov. An inversion formula for the attenuated x-ray transformation. *Ark. Mat.*, 40(1):145–167, 2002.
- [21] V. Ntziachristos and R. Weissleder. Experimental three-dimensional fluorescence reconstruction of diffuse media by use of a normalized born approximation. *Opt. Lett.*, 26:893895, 2001.
- [22] A. N. Panchenko. Inverse source problem of radiative transfer: A special case of the attenuated radon transform. *Inverse Problems*, 9:321337, 1993.
- [23] E.T. Quinto. Singularities of the x-ray transform and limited data tomography in \mathbb{R}^2 and \mathbb{R}^3 . *SIAM J. Math. Anal.*, 24:1215–1225, 1993.
- [24] M. Reed and B. Simon. *Methods of Modern Mathematical Physics I: Functional Analysis*. Academic Press, New York, 1972.
- [25] M. Reed and B. Simon. *Methods of Modern Mathematical Physics III*. Academic Press, New York, 1979.
- [26] V. A. Sharafutdinov. Inverse problem of determining a source in the stationary transport equation on a riemannian manifold. *Mat. Vopr. Teor. Rasprostr. Voln.*, 26:236–242, 1997.
- [27] C.E. Siewert. An inverse source problem in radiative transfer. *J. Quant. Spect. Radiat. Transfer*, 50:603–609, 1993.
- [28] P. Stefanov and G. Uhlmann. Optical tomography in two dimensions. *Methods Appl. Anal.*, 10:209–219, 2003.
- [29] P. Stefanov and G. Uhlmann. An inverse source problem in optical molecular imaging. *Analysis and PDE*, 1(1):115–126, 2008.
- [30] F. Trèves. *Introduction to Pseudodifferential and Fourier Integral Operators*, volume 1-2 of *The University Series in Mathematics*. Springer, 1980.
- [31] R. Weissleder and U. Mahmood. Molecular imaging. *Radiology*, 219:316333, 2001.
- [32] R. Weissleder, C.H. Tung, U. Mahmood, and A. Bogdanov. In vivo imaging of tumors with protease-activated near-infrared fluorescent probes. *Nature Biotechnology*, 17:375378, 1999.

DEPARTMENT OF MATHEMATICS, UNIVERSITY OF WASHINGTON, SEATTLE, WA 98195
E-mail address: `hubenjm@math.washington.edu`